Heat flow model for pulsed laser melting and rapid solidification of ion implanted GaAs

Taeseok Kim,[1,a)] Manoj R. Pillai,[2] Michael J. Aziz,[2] Michael A. Scarpulla,[3]
Oscar D. Dubon,[4] Kin M. Yu,[5] Jeffrey W. Beeman,[5] and Mark C. Ridgway[6]

[1]Solar Cell Technology and Development Group, SunPower Corporation, San Jose, California 95134, USA
[2]Harvard School of Engineering and Applied Sciences, Cambridge, Massachusetts 02138, USA
[3]Department of Electrical and Computer Engineering, Department of Materials Science and Engineering,
University of Utah, Salt Lake City, Utah 84112-9206, USA
[4]Department of Materials Science and Engineering, Lawrence Berkeley National Laboratory,
University of California, Berkeley, California 94720, USA
[5]Lawrence Berkeley National Laboratory, Berkeley, California 94720, USA
[6]Department of Electronic Materials Engineering, Research School of Physical Sciences and Engineering,
Australian National University, Canberra ACT 0200, Australia

In order to further understand the pulsed-laser melting (PLM) of Mn and N implanted GaAs, which we have used to synthesize thin films of the ferromagnetic semiconductor $Ga_{1-x}Mn_xAs$ and the highly mismatched alloy GaN_xAs_{1-x}, we have simulated PLM of amorphous (a-) and crystalline (c-) GaAs. We present a numerical solution to the one-dimensional heat equation, accounting for phase-dependent reflectivity, optical skin depth, and latent heat, and a temperature-dependent thermal conductivity and specific heat. By comparing the simulations with experimental time-resolved reflectivity and melt depth versus laser fluence, we identify a set of thermophysical and optical properties for the crystalline, amorphous, and liquid phases of GaAs that give reasonable agreement between experiment and simulation. This work resulted in the estimation of thermal conductivity, melting temperature and latent heat of fusion of a-GaAs of 0.008 W/cm K at 300 K, 1350 K, and 2650 J/cm^3, respectively. These materials properties also allow the prediction of the solidification velocity of crystalline and ion-amorphized GaAs. © 2010 American Institute of Physics. [doi:10.1063/1.3457106]

I. INTRODUCTION

Pulsed-laser melting (PLM) has been studied as a powerful technique to remove implantation damage in Si and GaAs since the 1980s. Early studies[1–6] pointed out that GaAs is highly sensitive to surface damage during the PLM process largely due to arsenic loss. Damage can be drastically reduced or eliminated by employing shallow ion implantation followed by PLM with laser fluence just sufficient to melt through the implanted damaged layer using spatially homogenized lasers in the UV, where the absorption coefficients α is quite large.

Highly mismatched semiconductor alloys (HMAs) have become important due to their dramatic changes in electronic properties from the host materials with just a small amount of alloying, which suggests many potential technological applications.[7] GaN_xAs_{1-x} is a HMA known especially for its large band gap reduction or bowing of 180 meV per x = 0.01 up to a few percent N.[8,9] Ferromagnetic semiconductors (FMSs) are of interest for use in magnetoelectronic or spintronic applications.[10–13] In systems such as $Ga_{1-x}Mn_xAs$, this coupling is mediated by holes and can result in relatively high T_C up to 170 K for $Ga_{1-x}Mn_xAs$ with x near 0.08.[14] Because the equilibrium solubility limits at room temperature for N and Mn in GaAs are lower than the atomic percent levels of interest for both of these alloy systems, kinetically-

controlled synthesis such as low temperature molecular beam epitaxy (LT-MBE) or ion implantation and PLM (II-PLM) are required for film synthesis.

The extremely fast melting and solidification rate in the PLM process result in highly supersaturated, substitutional solid solutions[15] giving rise to a large band gap reduction (HMA) or high T_C (FMS), comparable to those found in alloys produced by conventional thin film growth methods.

We have demonstrated II-PLM as a synthesis method for III-Mn-V FMSs like $Ga_{1-x}Mn_xAs$ with T_C above 135 K and $Ga_{1-x}Mn_xP$ with T_C up to 65 K,[14,16–19] and III-N-V HMAs like GaN_xAs_{1-x}.[20] $Ga_{1-x}Mn_xAs$ films produced using II-PLM do not exhibit signs of ferromagnetic second phases and exhibit structural, magnetic, and magnetotransport properties in quantitative agreement with those of films grown by LT-MBE.[21] In II-PLM synthesis of $Ga_{1-x}Mn_xAs$, GaAs wafers are ion implanted with Mn^+ creating a supersaturated concentration up to $5 \times 10^{21}/cm^3$ of Mn due to negligible bulk diffusion at room temperature. The transient heat flow resulting from the near-surface ($1/\alpha \sim 5$ nm) absorption of a single pulse from a high-powered UV laser is then used to melt through the implantation-induced structural damage (~ 100 nm). As heat is extracted into the substrate, a process of epitaxial solidification occurs with the crystal-melt interface returning to the surface at growth speeds of typically 1–10 m/s.[22] In II-PLM, the metastable $Ga_{1-x}Mn_xAs$ phase is achieved by this rapid solidification from the melt and sub-

a)Electronic mail: taeseok.kim@sunpowercorp.com.

108, 013508-1

sequent quenching at rates up to 10^{10} K/s.[23] Incorporation of dopants at concentrations up to hundreds of times the room temperature equilibrium solubility limit is routinely achieved using II-PLM.[24-27]

By similar methods, we have produced thin films of GaN_xAs_{1-x}, and analysis by photomodulated reflectance[20] and ballistic electron emission spectroscopy[28,29] show ~180 meV decrease per atomic percent N in both band gap and Schottky barrier height for dilute nitrogen incorporation.

PLM has been studied extensively in crystalline Si (Refs. 15 and 30) including modeling of the heat flow governing the solidification process.[31] The melting and solidification during PLM occurs on ns time scales, while the absorption of photons and their conversion to heat occurs on faster time scales.[24] This allows the heat deposition due to the laser pulse to be described spatially by the absorption of the appropriate optical stack and temporally by the laser pulse itself. For large area samples and irradiation below the ablation threshold, a one-dimensional (1D) heat flow model is appropriate. The heat deposited by the laser will cause some portion of the sample to melt and then solidify as heat subsequently flows into the substrate. For simulations of melting of an ion amorphized semiconductor layer on a crystalline substrate, it is necessary to incorporate the optical and thermophysical properties of the crystalline, amorphous, and liquid phases. In order to better understand and refine PLM processing for $Ga_{1-x}Mn_xAs$ and GaN_xAs_{1-x}, we have simulated the melting and solidification during PLM of ion implanted GaAs. Many of the thermophysical properties required for the liquid and amorphous phases of GaAs are not well known; thus this work comparing simulation to experiment represents independent estimates of some of these values.

II. EXPERIMENT

In order to investigate PLM of ion amorphized layers, semi-insulating GaAs (001) wafers were implanted with $^{40}Ar^+$ at multiple energies. Ar^+ was implanted at 180, 80, and 35 keV to doses of (respectively) 5×10^{15}, 1.5×10^{15}, and $7 \times 10^{14}/cm^2$. Each sample was irradiated in air with a single pulse from a XeCl excimer laser [$\lambda = 308$ nm, 30 ns full width at half maximum (FWHM)]. A multiprism homogenizer was used to produce a spatially uniform fluence ranging between 0.04 and 0.61 J/cm^2 over the sample area of approximately 5×5 mm^2. The uncertainty in the fluence of each XeCl laser pulse is estimated at 10%. A low-power continuous wave 488 nm argon ion laser beam was focused on the sample in the center of the XeCl spot to <1 mm diameter and used to monitor the time-resolved reflectivity (TRR) of the samples during the excimer laser irradiation. The 488 nm beam was detected by a fast Si diode and captured by a digitizing oscilloscope triggered off the XeCl beam using a second diode.[1] Melting of the sample surface by the XeCl laser was detected by an abrupt increase in the sample reflectivity indicating a more reflective liquid phase, as shown in Fig. 1.[1,31]

A finite differences code using explicit forward Euler time steps based on the LASER code was used with
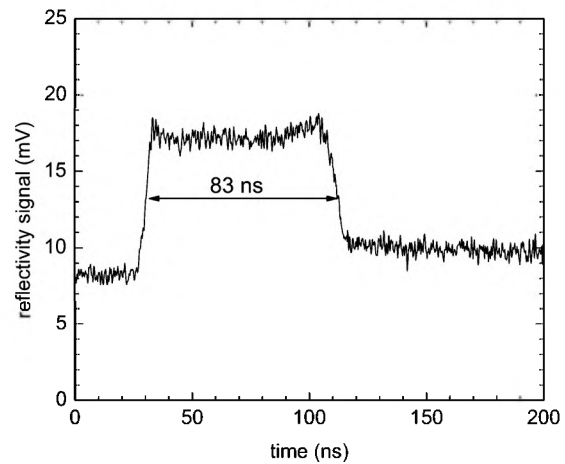

FIG. 1. Typical reflectivity measurement for a c-GaAs sample.

temperature-dependent thermophysical properties to simulate the 1D heat flow resulting from laser irradiation.[32] Materials properties are input to the program from a file including temperature dependent properties, which are interpolated linearly during the calculation. The measured time-dependent intensity of the XeCl pulse is used to determine the heat deposition by absorption. The following nucleation and growth rules are applied in the current simulation. In a case of incomplete melting of an amorphous material, the amorphous material is assumed to regrow as an amorphous solid or as a crystalline solid for comparison. In a case of fully melting the amorphous layer resulting in a crystal/liquid interface, the liquid is assumed to regrow as a crystalline solid, as reported previously.[14,16-20,28,29]

Overheating and undercooling are allowed for by determining the position of the liquid-solid interface from

$$\nu = \mu(T - T_m), \tag{1}$$

where ν is the interface velocity, μ is the kinetic undercooling coefficient, T is the interface temperature, and T_m is the equilibrium melting temperature of pure GaAs. μ is a property of the crystalline-melt interface and a value of 0.0667 m/s K has been shown to be appropriate for (001) Si in previous work.[32] To obtain a value for GaAs in this study, we scaled this value by the ratios of T_m and latent heat of fusion[33] for crystalline (c-) GaAs and c-Si as shown in Table II; this was found to give satisfactory results. Variations in μ by factors of 2 about this value do not significantly affect the results. It is found that nearly-negligible undercooling and superheating gave melt depths and durations consistent with our experiments for the liquid-crystal GaAs interface, i.e., the interface velocity is determined mainly by heat flow in the sample, with the interface tracking closely the T_m isotherm.

III. RESULTS AND DISCUSSION

At the lowest fluences, surface melting does not occur and only photogenerated carriers contribute to the increase in reflectivity. Melting of the GaAs surface occurs above a threshold fluence, which we estimate to be near 0.08 J/cm^2 for amorphous (a-) GaAs and 0.2 J/cm^2 for c-GaAs even

though the measurement of the threshold fluence has been known to be limited by the surface conditions such as an inhomogeneous melting and surface contamination.[34] Figure 1 shows a representative TRR trace obtained for irradiation of c-GaAs at 0.34 J/cm^2. The melt duration (τ_{melt}) was experimentally determined to be 83 ns using the FWHM of the reflectivity change. The formation of a liquid phase at the surface is indicated by the rapid rise in reflectivity as the XeCl pulse is absorbed by the sample. Because the absorption length of the 488 nm Ar$^+$ laser in liquid GaAs is less than the depth of melting, TRR shows a flat-topped profile until the solidification front returns to within the absorption depth, as indicated by the relatively abrupt drop in reflectivity. The abruptness of the trailing edge is an indication of the planar character of the solidification front, which can be lost by pump laser inhomogeneities or cellular breakdown during solidification.

For implant-amorphized samples, beyond the fluence threshold for the onset of melting, another fluence threshold exists above which the entire amorphous layer is melted and solidification proceeds from the undamaged crystalline semiconductor below. This threshold fluence for complete melting depends primarily on the implant-damaged layer thickness and the temporal pulse shape and wavelength of the laser. High quality single-crystalline epitaxial regrowth occurs under these conditions; this is the regime in which we have synthesized our films of Ga$_{1-x}$Mn$_x$As and GaN$_x$As$_{1-x}$ in prior work.

For fluences in between these two thresholds, the primary melt does not fully consume the amorphous layer and polycrystalline solidification appears to nucleate from the liquid-amorphous interface. Because the latent heat of the liquid-crystalline transition exceeds that of the liquid-amorphous transition and the thermal diffusivity in the amorphous phase is relatively low, the latent heat released during crystallization of the liquid is sufficient to rapidly launch a melting front into the underlying amorphous layer which then solidifies in a phenomenon known as explosive crystallization.[35,36] As a result, the formation of a fine-grained polycrystalline (FP) explosive crystalline region beneath a large-grained polycrystalline (LP) regrowth region has been observed in cross sectional transmission electron microscopy (XTEM).[36]

Figure 2 shows a cross XTEM image of a GaAs sample Ar$^+$ implanted and rradiated at 0.12 J/cm^2, a fluence above the surface melting threshold but below the complete melting threshold. The topmost region is a LP GaAs, under which is found a layer of FP GaAs spanning depths from about 75 to 160 nm. No a-GaAs remains, as the inset shows the interface between the FP region and the c-GaAs substrate with atomic resolution. We used the depth of this FP/c-GaAs boundary as the initial thickness of the a-GaAs for the heat flow simulation in this study. Within the c-GaAs region, dislocations rings and voids at the end of the implantation profile appear similar to those in the previous study.[20]

TRR data similar to those in Fig. 1 were used to determine τ_{melt} over a range of fluences for both Ar$^+$ implanted GaAs and unimplanted c-GaAs. These data are displayed in Fig. 3(a) as the discrete data points. It is immediately appar-
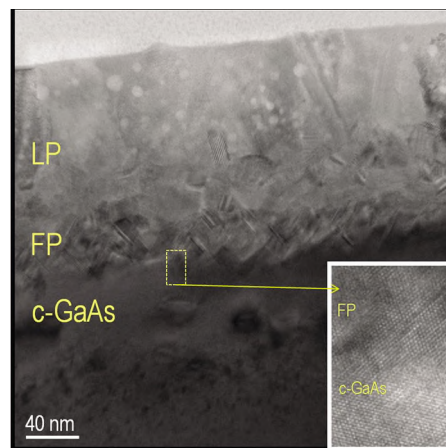

FIG. 2. (Color online) XTEM image of the Ar$^+$ implanted GaAs melted at 0.12 J/cm^2. The image shows two regrown GaAs regions; LP and FP GaAs. Note that the FP GaAs extends to the original amorphous-crystalline interface as shown in the inset at the boundary. Bubbles visible in the LP region are believed to be bubbles of the argon implant that have nucleated during heating from ion milling.

ent that the surface melting of c-GaAs requires greater XeCl fluence; the thresholds for surface melting are estimated to be near 0.08 J/cm^2 and 0.2 J/cm^2 for ion-implanted and crystalline samples, respectively. The experimental data point labeled "LP" in Fig. 3(b) is the depth of the primary melt depth and was obtained from the XTEM observation of the Ar$^+$ implanted sample irradiated at 0.12 J/cm^2 as shown by the LP region in Fig. 2. The lines in Fig. 3 are the results of the simulations undertaken in this work and are seen to be in reasonable agreement with the experimental data. The dashed line for a-GaAs is the result using a different nucleation rule, where the liquid GaAs regrows as a crystalline solid at all fluences. The higher thermal conductivity of c-GaAs resulted in shorter melt durations, resulting in a deviation from the measured values. Because the simulation does not include the complexities associated with explosive crystallization, e.g., the multiple simultaneous liquid/crystal interfaces, we do not expect the simulations to model well the temporal behavior below the threshold for fully melting the amorphous layer.

Accurate simulation of the heat generation, heat flow, and melting of GaAs requires the knowledge of many materials properties: the heat capacity (C_P), the thermal conductivity (κ), the optical reflectivity for normal incidence (R), and the optical absorption coefficient (α), are all required for the crystalline, amorphous, and liquid phases. The melting temperatures and latent heats for the crystal/liquid and amorphous/liquid phase changes are also required. As the mass density and C_P always appear together in the heat diffusion equation, the density is bundled into C_P which is thus presented as a volume-denominated quantity. The temperature dependent density data for GaAs from Ref. 37 were fit to the empirical polynomial, $\rho(T) = -8.2917 \times 10^{-9}$ T^2 - 8.5624 $\times 10^{-5}$ T + 5.3429 where ρ is in gram per cubic centimeter and T is in K. Temperature dependent C_P and κ data are available for the crystalline phase at many doping levels; as the wafers in this study were semi-insulating data for the lowest doping level were chosen. The C_P data above 200 K
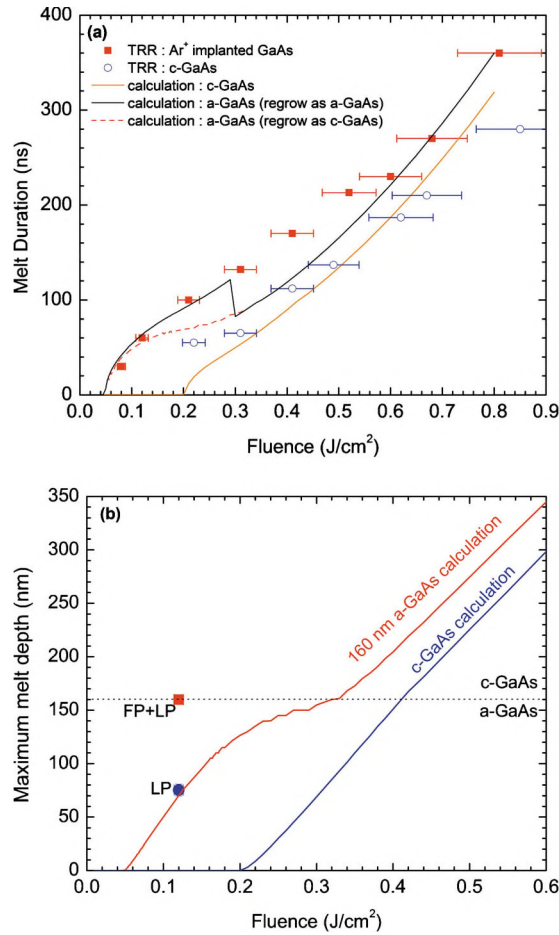
FIG. 3. (Color online) Experimental τ_{melt} (a) and melt depth (b) (discrete points) plotted with predictions from the heat flow simulations described in the text (lines). In (a), τ_{melt} is measured from TRR of c-GaAs or Ar$^-$ implanted, amorphized GaAs. The different assumptions for the two a-GaAs curves are discussed in the text. In (b), the thickness of the LP region from the XTEM in Fig. 2 is assigned as the primary melt depth (LP), and the FP+LP is used to identify the original implantation-induced amorphized thickness. The FP region is believed to be caused by the explosive crystallization.

TABLE I. Thermal conductivity (κ) and volumetric heat capacity (C_P) for c-GaAs used in this work.

Temperature (K)	κ (W/cm K)	Temperature (K)	C_P (J/K cm^3)
266	0.558	212	1.74
288	0.526	300	1.78
308	0.477	400	1.82
437	0.293	500	1.87
462	0.28	600	1.92
494	0.256	700	1.97
524	0.238	800	2.01
601	0.208	900	2.06
683	0.175	1000	2.11
782	0.148	1100	2.15
869	0.131	1200	2.20
986	0.113	1300	2.24
1500	0.07	1400	2.29
3000	0.032	1500	2.34
6000	0.017	3000	2.34
8000	0.011	6000	2.34
		8000	2.34

on surface contamination, composition, roughness, etc., so our determined values should be regarded as guidelines as opposed to exact values or the previously known dielectric functions measured without involving melting and solidification phenomena.[42]

Having determined the properties of the crystalline and liquid phases, it was necessary to determine many of the properties of ion-amorphized GaAs by finding agreement in simulations with the measured melt depth and duration data in Fig. 3. The crystalline value of C_P was used because the slightly higher C_P due to greater entropy in the amorphous phase[43] should cancel the presumed slightly lower density of the ion-amorphized phase when C_P is expressed in volumetric units. If this cancellation does not occur, for example, if the density of the amorphous phase is slightly greater than that of the crystalline phase, it is expected that any deviation from the crystalline value would be at the 10% level. While the variation in the heat of crystallization for a-Si for the different states of relaxation has been studied well,[44] the PLM experiments and the heat flow simulation on a-Si has also shown the insensitivity of this variation to the prediction of the thermodynamic properties of a-Si during PLM.[15] For the case of GaAs, we have no reason to expect this to change significantly. We also recognize that in principle the relaxation state can depend on implant species, but we have no evidence that this dependence is significant. Related to this

the data from Refs. 38 and 37 were averaged to give continuity with the low temperature data. This data set was in reasonable agreement with the values used by Jordan.[39] At low temperatures, the κ values from Ref. 40 were used while at high temperatures values were taken from Ref. 38. This composite data set was in reasonable agreement with the values from Refs. 37 and 39. Table I presents the temperature dependent C_P and κ used for the c-GaAs in this work. The equilibrium melting temperature (T_m) and latent heat of fusion (ΔH_m) are properties of the crystalline-liquid phase transition and are presented in Table II. Values for the liquid GaAs phase of $C_P = 2.49$ J cm^{-3} K^{-1}, $\kappa = 0.178$ W cm^{-1} K^{-1}, and 5.72 g/cm^3 were taken from Ref. 39 and were in agreement with those from Ref. 41.

The optical properties of c- and liquid (l-) GaAs were taken from Ref. 37 but the reflectivity of l-GaAs (R_L) was adjusted for the heat flow simulation to give the best agreement with the experimental melt duration of c-GaAs PLM at the XeCl wavelength (308 nm) as shown in Fig. 3(a); values of R_L and R_C from this initial calibration are 0.46 and 0.41, respectively. These reflectivities are likely to be dependent

TABLE II. Values used in this work for the equilibrium melting temperature (T_m), latent heat (ΔH_m), and kinetic undercooling coefficient for the crystal-liquid and amorphous-liquid phase transitions.

Thermal properties	Crystalline-liquid	Amorphous-liquid
Melting temperature, T_m (K)	1511[a]	1350[b]
Latent heat of fusion, ΔH_m (J/cm^3)	3783[a]	2648[b]
Kinetic undercooling, μ [(m/s)/K]	0.0747[b]	0.0747[b]

[a]Reference 37.
[b]Reference 54.

TABLE III. Optical properties used in this study for amorphous, crystalline, and liquid GaAs.

Optical properties	Crystalline	Amorphous	Liquid
Optical reflectivity at 308 nm	0.41[a]	0.43 (this study)	0.46 (this study)
Optical absorption coefficient at 308 nm (1/cm)	0.79×10^6 [a]	1.0×10^6 [b]	0.83×10^6 [b]

[a]Reference 37.
[b]Reference 54.

point, we observed an insignificant dependence of the melt duration on implanted nitrogen dose over the range 1.0×10^{15} to $5.0 \times 10^{15}/\text{cm}^2$ in previous study,[45] where the upper guide line for fully ion-amorphized GaAs was generated using the parameters in the paper. The optical absorption coefficient of ion amorphized GaAs, was obtained from the data in Ref. 46. The reflectivity value of a-GaAs (R_a) of 0.43 at 308 nm predicted a surface melting threshold of the a-GaAs in good agreement with the experimental value as shown in Fig. 3(a) but again should be considered a guideline (Table III).

Finally, the temperature dependent κ values for the amorphous phase were determined by making an assumption and testing with the experimental melt duration in Fig. 3(a). The assumption was motivated by the hypothesis that the temperature dependence of the thermal conductivities of amorphous semiconductors would be relatively similar. We started from the known temperature dependence of κ for amorphous Si (Ref. 47) and offset the equation to give the best fit for our experimental result. The best fit in the incomplete fluence region was done with the a-GaAs thermal conductivity of 0.008 W/cm K at 300 K. The thermal conductivity of a-Ge should be very close to that of a-GaAs and has been reported in the range from 0.004 to 0.010 W/cm K at 300 K depending on the measured film thicknesses and the deposition techniques.[48]

The solidification velocity is the most important parameter governing impurity incorporation during PLM (crystalline orientation is also relevant[49]); however, it is one of the more inaccessible parameters experimentally.[15,50–52] In general, faster solidification will lead to incorporation of dopants at higher concentrations;[15] in the case of N in $\text{GaN}_x\text{As}_{1-x}$, this should translate into larger band gap reduction and in the case of Mn in $\text{Ga}_{1-x}\text{Mn}_x\text{As}$, into higher T_c. Numerical simulations allow the estimation of the solidification velocity to be explored as a function of any number of PLM parameters. Figure 4 presents the simulated melt depth versus time at different laser fluences for the bulk c-GaAs, Fig. 4(a), and a-GaAs/c-GaAs samples, Fig. 4(b), by using the material parameters and the XeCl laser used in this study. The interface velocities in the insets are given simply by the slopes of the depth versus time curves. The maximum velocity occurs near the beginning of solidification at the maximum melt depth and the solidification front decelerates as it approaches the surface due to the thermal gradient which decreases over time as shown in the inset of each figure. Note that the solidification velocities are lower for greater depths of melting. As solute trapping increases with interface velocity,[15] this indicates that the highest concentration $\text{Ga}_{1-x}\text{Mn}_x\text{As}$ and $\text{GaN}_x\text{As}_{1-x}$ films may be synthesized by irradiating the shallowest possible ion-implants at the threshold for fully melt-

ing the ion damage. Figure 5 summarizes the maximum solidification velocities predicted for the bulk c-GaAs (solid squares) and the 160 nm a-GaAs/c-GaAs (open circles) at various fluences by using the simulation parameters determined in this study. The abrupt change for the a-GaAs at around 0.28 J/cm² is an artifact the heat flow simulation where the amorphous-crystalline interface is assumed to be abrupt. In these simulations, maximum velocities of typically 3–4 m/s are predicted for solidification of GaAs after irradiation with this fairly typical XeCl laser. This is slower than solidification in Si, which is predicted at 5–6 m/s using the same simulation code, due to the lower thermal conductivity of GaAs; however it is still to be determined whether this slower solidification corresponds to less efficient solute trap-
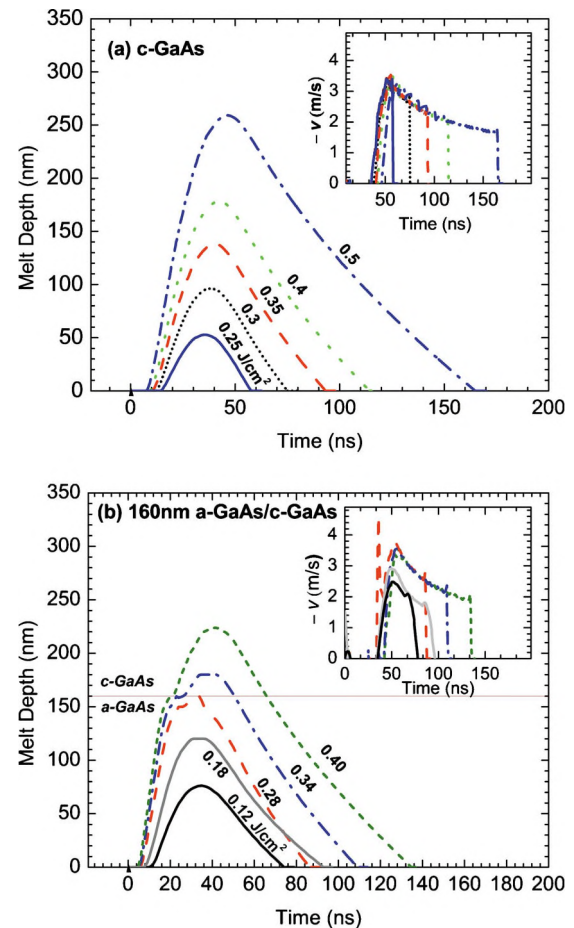

FIG. 4. (Color online) Simulated melt depths vs time for bulk c-GaAs (a) and the a-GaAs (b) at various fluences by using the parameters determined in this study. The inset in each figure shows the solidification velocity vs time at different fluences. The color and the shape of each line in the melt depth-time and the solidification velocity-time plot are coded by different laser fluences in the same way. The abrupt drop to zero velocity for each curve indicates the point at which the surface solidifies.
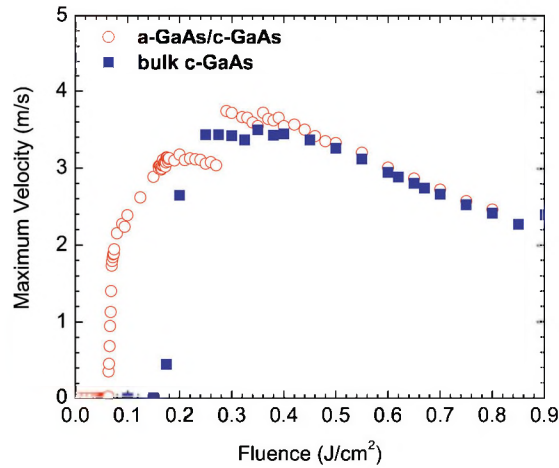
FIG. 5. (Color online) The maximum instantaneous solidification velocity predicted for the bulk c-GaAs (solid squares) and the 160 nm a-GaAs/c-GaAs (open circles) at various fluences by using the simulation parameters determined in this study.

ping. It is clear that in $Ga_{1-x}Mn_xAs$, $10^{21}/cm^3$ ferromagnetically active Mn and Te donors can be incorporated using II-PLM,[16,17,19,53] which is comparable to the concentrations of active dopants achievable in II-PLM of Si.[24–27] Note that these single-crystalline epitaxial growth rates are approximately 10^5 times faster than MBE or organometallic vapor phase epitaxy growth and 10^{10} times faster than Czochralski growth of bulk single crystals.

IV. CONCLUSIONS

In summary we have developed a set of estimated numerical values for the materials properties for the crystalline, ion-implantation-amorphized, and liquid phases of GaAs appropriate for simulating the PLM process and used them to estimate the solidification velocities during PLM. This work resulted in the estimation of melting temperature, latent heat of fusion, and the thermal conductivity of a-GaAs to be 1350 K, 2650 J/cm^3, and 0.008 W/cm K at 300 K, respectively. The 308 nm reflectivities of amorphous and liquid GaAs were determined to be 0.43 and 0.46. These materials properties give reasonable agreement with TRR and melt depth data for XeCl PLM of crystalline and ion-amorphized GaAs and allow the prediction of difficult to measure parameters such as the solidification velocity, which controls the concentration of dopants incorporated during solidification.

ACKNOWLEDGMENTS

[1]D. H. Lowndes and R. F. Wood. Appl. Phys. Lett. **38**. 971 (1981).

[2]D. E. Davies. J. P. Lorenzo. and T. G. Ryan. Appl. Phys. Lett. **37**. 612 (1980).

[3]J. Fletcher. J. Narayan. and D. H. Lowndes. Mater. Res. Soc. Symp. Proc. **2**. 421 (1981).

[4]J. S. Williams. R. G. Elliman. W. L. Brown. and T. E. Seidel. Phys. Rev. Lett. **55**. 1482 (1985).

[5]D. H. Lowndes. R. F. Wood. and J. Narayan. Phys. Rev. Lett. **52**. 561 (1984).

[6]J. S. Williams and H. B. Harrison. in *Laser and Electron-Beam Solid Interactions*. edited by L. D. H. J. F. Gibbons and T. W. Sigmon (Elsevier/North-Holland. New York/Amsterdam. 1981). pp. 209–222.

[7]J. W. Ager and W. Walukiewicz. Semicond. Sci. Technol. **17**. 741 (2002).

[8]K. Uesugi. N. Morooka. and I. Suemune. Appl. Phys. Lett. **74**. 1254 (1999).

[9]M. Kondow. K. Uomi. K. Hosomi. and T. Mozume. Jpn. J. Appl. Phys., Part 2 **33**. L1056 (1994).

[10]S. A. Wolf. D. D. Awschalom. R. A. Buhrman. J. M. Daughton. S. von Molnár. M. L. Roukes. A. Y. Chtchelkanova. and D. M. Treger. Science **294**. 1488 (2001).

[11]S. A. Wolf. A. Y. Chtchelkanova. and D. M. Treger. IBM J. Res. Dev. **50**. 101 (2006).

[12]G. A. Prinz. Science **282**. 1660 (1998).

[13]H. Ohno. Science **281**. 951 (1998).

[14]P. R. Stone. M. A. Scarpulla. R. Farshchi. I. D. Sharp. E. E. Haller. O. D. Dubon. K. M. Yu. J. W. Beeman. E. Arenholz. J. D. Denlinger. and H. Ohldag. Appl. Phys. Lett. **89**. 012504 (2006).

[15]M. J. Aziz. Metall. Mater. Trans. A **27**. 671 (1996).

[16]M. A. Scarpulla. U. Daud. K. M. Yu. O. Monteiro. Z. Liliental-Weber. D. Zakharov. W. Walukiewicz. and O. D. Dubon. Physica B **340–342**. 908 (2003).

[17]M. A. Scarpulla. O. D. Dubon. K. M. Yu. O. Monteiro. M. R. Pillai. M. J. Aziz. and M. C. Ridgway. Appl. Phys. Lett. **82**. 1251 (2003).

[18]M. A. Scarpulla. B. L. Cardozo. R. Farshchi. W. M. Hlaing Oo. M. D. McCluskey. K. M. Yu. and O. D. Dubon. Phys. Rev. Lett. **95**. 207204 (2005).

[19]O. D. Dubon. M. A. Scarpulla. R. Farshchi. and K. M. Yu. Physica B **376–377**. 630 (2006).

[20]K. M. Yu. W. Walukiewicz. M. A. Scarpulla. O. D. Dubon. J. Wu. J. Jasinski. Z. Liliental-Weber. J. W. Beeman. M. R. Pillai. and M. J. Aziz. J. Appl. Phys. **94**. 1043 (2003).

[21]M. Scarpulla. R. Farshchi. P. R. Stone. R. V. Chopdekar. K. M. Yu. Y. Suzuki. and O. D. Dubon. J. Appl. Phys. **103**. 073913 (2008).

[22]J. M. Poate. Mater. Res. Soc. Symp. Proc. **4**. 121 (1982).

[23]P. Baeri. Mater. Sci. Eng., A **178**. 179 (1994).

[24]M. von Allmen and A. Blatter. *Laser-Beam Interactions with Materials: Physical Principles and Applications*. 2nd ed. (Springer. Berlin. 1995).

[25]C. W. White. B. R. Appleton. and S. R. Wilson. in *Laser Annealing of Semiconductors*. edited by J. M. Poate and J. W. Mayer (Academic. New York. 1982). pp. 112–145.

[26]C. W. White. in *Pulsed Laser Processing of Semiconductors*. edited by R. F. Wood. C. W. White. and R. T. Young (Academic. Orlando. 1984). pp. 44–92.

[27]C. W. White. S. R. Wilson. B. R. Appleton. and F. W. Young. J. Appl. Phys. **51**. 738 (1980).

[28]T. Kim. M. J. Aziz. and V. Narayanamurti. Appl. Phys. Lett. **93**. 102117 (2008).

[29]T. Kim. K. Alberi. O. D. Dubon. M. J. Aziz. and V. Narayanamurti. J. Appl. Phys. **104**. 113722 (2008).

[30]J. A. Kittl. P. G. Sanders. M. J. Aziz. D. P. Brunco. M. O. Thompson. Acta Mater. **48**. 4797 (2000).

[31]P. Baeri and S. U. Campisano. in *Laser Annealing of Semiconductors*. edited by J. M. Poate and J. W. Mayer (Academic. London. 1982). p. 75.

[32]D. E. Hoglund. M. O. Thompson. and M. J. Aziz. Phys. Rev. B **58**. 189 (1998).

[33]D. Turnbull. in *Thermodynamics in Physical Metallurgy* (American Society for Metals. Cleveland. 1950). pp. 282–306.

[34]J. Solis. C. N. Afonso. and J. Piqueras. J. Appl. Phys. **71**. 1032 (1992).

[35]J. Narayan. C. W. White. O. W. Holland. and M. J. Aziz. J. Appl. Phys. **56**. 1821 (1984).

[36]M. O. Thompson. G. J. Galvin. J. W. Mayer. P. S. Peercy. J. M. Poate. D. C. Jacobson. A. G. Cullis. and N. G. Chew. Phys. Rev. Lett. **52**. 2360 (1984).

[37]M. R. Brozel and G. E. Stillman. *Properties of Gallium Arsenide*. 3rd ed.,

EMIS Data Reviews Series No. 16 (INSPEC—The Institution of Electrical Engineers, London, 1996).

[38] J. S. Blakemore, J. Appl. Phys. **53**, R123 (1982).

[39] A. S. Jordan, J. Cryst. Growth **71**, 551 (1985).

[40] R. O. Carlson, G. A. Slack, and S. J. Silverman, J. Appl. Phys. **36**, 505 (1965).

[41] S. Nakamura and T. Hibiya, Int. J. Thermophys. **13**, 1061 (1992).

[42] A. M.-T. Kim, J. P. Callan, C. A. D. Roeser, and E. Mazur, Phys. Rev. B **66**, 245203 (2002).

[43] R. Zallen, *The Physics of Amorphous Solids* (Wiley, New York, 1983).

[44] S. Roorda, W. C. Sinke, J. M. Poate, D. C. Jacobson, S. Dierker, B. S. Dennis, D. J. Eaglesham, F. Spaepen, and P. Fuoss, Phys. Rev. B **44**, 3702 (1991).

[45] T. Kim, *Electrical and Optical Characterization and Nanoscale Patterning of Gallium Nitrogen Arsenide Synthesized by Energetic Beams* (Harvard University, Cambridge, 2008).

[46] J. Stuke and G. Zimmerer, Phys. Status Solidi B **49**, 513 (1972).

[47] H. C. Webber, A. C. Cullis, and N. G. Chew, Appl. Phys. Lett. **43**, 669 (1983).

[48] D. Cahill, H. E. Fischer, T. Klitsner, E. T. Swartz, and R. O. Pohl, J. Vac. Sci. Technol. A **7**, 1259 (1989).

[49] R. Reitano, P. M. Smith, and M. J. Aziz, J. Appl. Phys. **76**, 1518 (1994).

[50] D. M. Hsieh, J. Y. Wang, and A. Y. G. Fuh, Jpn. J. Appl. Phys., Part 2 **36**, L455 (1997).

[51] B. J. Keay, M. Mendenhall, and G. S. Edwards, Phys. Rev. B **60**, 10898 (1999).

[52] M. O. Thompson, J. W. Mayer, A. G. Cullis, H. C. Webber, N. G. Chew, J. M. Poate, and D. C. Jacobson, Phys. Rev. Lett. **50**, 896 (1983).

[53] P. A. Barnes, H. J. Leamy, J. M. Poate, S. D. Ferris, J. S. Williams, and G. K. Celler, Appl. Phys. Lett. **33**, 965 (1978).

[54] M. A. Scarpulla, *III-Mn-V Ferromagnetic Semiconductor Synthesized by Ion Implantation and Pulsed-Laser-Melting* (University of California, Berkeley, 2006).